Journal of Biomolecular NMR, **12:** 73–88, 1998.
KLUWER/ESCOM

Internal and overall motions of the translation factor eIF4E: Cap binding and insertion in a CHAPS detergent micelle

Abigail Manson McGuire, Hiroshi Matsuo and Gerhard Wagner*
Graduate Program in Biophysics and Department of Biological Chemistry and Molecular Pharmacology, Harvard Medical School, 240 Longwood Avenue, Boston, MA 02115, U.S.A.

Received 18 December 1997; Accepted 26 February 1998

Key words: 15^N relaxation, eIF4E, translation, dynamics

Abstract

The mRNA cap-binding protein eIF4E is the limiting factor in the eIF4F translation initiation complex, which mediates the binding of the 40S ribosome to the mRNA. ^{15}N relaxation studies have been used to characterize the backbone dynamics of deuterated eIF4E in a CHAPS micelle for the apoprotein, the m^{7}GDP-bound form, and the dinucleotide (m^{7}GpppA)-bound form, as well as for CHAPS-free eIF4E. Large differences in overall correlation time between the CHAPS-free form (11.8 ns) and samples containing different concentrations of CHAPS (15.9–19.4 ns) indicate that eIF4E is embedded in a large micelle in the presence of CHAPS, with a total molecular weight in the range of 40–60 kDa. CHAPS seems to restrict the mobility of the a2–b3 and a4–b5 loops which are thought to be embedded in the micelle. No significant changes in overall mobility were seen between the m^{7}GDP-bound form, the m^{7}GpppA-bound form, and the apoprotein. Amide hydrogen exchange data indicate the presence of slowly exchanging amides in two surface-exposed helices (a2 and a4), as well as the a4–b5 loop, indicating protection by the CHAPS micelle. The micelle covers the convex side of the protein away from the cap-binding site.

Introduction

Yeast eIF4E is a 213-residue protein which binds specifically to the mRNA 5′ cap structure. As the limiting factor in the eIF4F complex, consisting of eIF4A, 4E, and 4G (p220), eIF4E plays a key role in translation initiation regulation by phosphorylation and interaction with the 4E-binding proteins, 4E-BP1 and 4E-BP2 in humans, PHAS I in rat and p20 in yeast (Merrick et al., 1996). These homologous 4E-binding proteins inhibit translation in their unphosphorylated state by competitively binding to the eIF4G binding site on eIF4E (Haghighat et al., 1995). Recently, the structures of both mouse (Marcotrigiano et al., 1997) and yeast (Matsuo et al., 1997) eIF4E have been determined in complex with m^{7}GDP. The yeast eIF4E structure consists of a curved, eight-stranded, antiparallel β-sheet with three long and three short α-helices (see Figure 1a). The three long α-helices lie on the convex side of the β-sheet; a stack of tryptophans in the concave face forms the binding site for the mRNA cap. Figure 1b shows an ensemble of structures seen from the convex side, away from the cap-binding site. The N-terminal 35 residues are predominantly unstructured (Matsuo et al., 1997).

Yeast eIF4E is insoluble above ∼0.5 mM, which limits the sensitivity of NMR studies. Moreover, even at concentrations less than 0.5 mM, it precipitates over the course of several days. This can be alleviated by the addition of non-denaturing detergents. The best results for solubility and stability of yeast eIF4E were obtained with the addition of CHAPS (3-[(3-cholamidopropyl)dimethylammonio]-1-propanesulfonate hydrate). The addition of CHAPS causes spectral changes primarily of surface residues but the overall appearance of the NMR spectra is not changed, indicating that the structure is not changed significantly. No additional spectral changes are seen

*To whom correspondence should be addressed.

above ∼25 mM CHAPS. Adding 25–50 mM of CHAPS increases the solubility of yeast eIF4E to ca. 1 mM (Matsuo et al., 1997). The stability is also dramatically increased and no precipitation is observed for over 6 months. CHAPS has a critical micelle concentration of around 6 mM (Chattopadhyay and Harikumar, 1996); hence, at the CHAPS concentrations used here the eIF4E will be contained within a CHAPS micelle. Dynamic light scattering experiments using a sample with 25 mM CHAPS indicate a particle size of around 50 kDa; however, large baseline parameters indicate a high level of polydispersity (Matsuo et al., 1997). The structure of yeast eIF4E was determined in a CHAPS micelle (Matsuo et al., 1997).

The region of eIF4E embedded in the micelle was initially determined from a CHAPS titration experiment (Matsuo et al., 1997). The resonances that shift with the addition of CHAPS are located in a contiguous surface on one face of eIF4E, consisting of two long helices on the convex side of the protein away from the cap-binding site (a2 and a4), β-strands b1 and b2, and the loops connecting a2 to b3 and a4 to b5 (see Figures 1b and c). The cap-binding site is out of the micelle, which is consistent with the observation that the binding of cap analogs is not affected by the presence of CHAPS. The curvature of the CHAPS micelle tends to open up the cap-binding site slightly, causing the cap analog to associate more tightly with Trp^{104} than with Trp^{58} (Matsuo et al., 1997).

To understand how the CHAPS micelle affects the internal and overall mobility of eIF4E, we used two-dimensional heteronuclear relaxation techniques (Nirmala and Wagner, 1988,1989; Kay et al., 1989) and reduced spectral density mapping (Peng and Wagner, 1992a,b,1995; Ishima and Nagayama, 1995a,b) to characterize the backbone dynamics with varying concentrations of CHAPS. We compared the backbone dynamics of the m^7GDP-bound form, the m^7GpppA-bound form, and the apoprotein. We also performed amide hydrogen exchange experiments to characterize the solvent accessibility of eIF4E in the CHAPS micelle.

Materials and Methods

Expression and purification of eIF4E

The yeast eIF4E was subcloned into the pGEM.2 vector (Promega) and transformed into the Bl21 (DE3) *E. coli* strain (Novagen). Transformed cells were grown in minimal media with $^{15}NH_4Cl$ (1 g/l) and 99% D_2O. The yield on D_2O was typically 5 mg/l. After cell lysis using a French Press, eIF4E was bound to an m^7GDP-affinity resin and eluted with 0.2 mM m^7GDP (Edery et al., 1988). Samples were concentrated to ∼0.5 mM in 50 mM phosphate buffer, pH 6.5. For the samples containing CHAPS, 25–50 mM CHAPS was added immediately after concentration.

Making pure apoprotein turned out to be difficult, as the protein could not be eluted from the cap affinity column with high salt only. Therefore, a different procedure was used. The protein was eluted with m^7GDP and then dialyzed against high salt buffer (0.5 M potassium phosphate buffer, pH 6.5, and 0.5 M KCl). In the next step it was dialyzed again into low salt buffer. This dislodged most, but not all, of the bound m^7GDP, based on the presence in the HSQC spectra of small residual peaks at the chemical shifts for the m^7GDP-bound form. Thus, the 'apoprotein' sample probably retained a small fraction of residual m^7GDP. Whenever we talk about the apoprotein, we refer to protein made in this way.

To prepare a complex of yeast eIF4E with the dinucleotide m^7GpppA, the dinucleotide was added at high concentration (>1:1) to the apoprotein prepared as described above.

NMR spectroscopy

All experiments were recorded on a Varian Unity 500 spectrometer at 25 °C. Sensitivity-enhanced pulse sequences were used as described in Farrow et al. (1994). Heteronuclear ^1H-^{15}N NOE enhancements (XNOEs) were measured by taking the ratio of peak intensities in spectra recorded with (I_{sat}) and without (I_0) 5 seconds of presaturation ($XNOE = (I_{sat} - I_0)/I_0$). I_0 and I_{sat} were measured with a 6 s recycle delay. The presaturation delay of 5 s is approximately $5 \times T_1$ for most, but not all, ^{15}N nuclei of the protein, and the steady-state heteronuclear NOE may be slightly underestimated for some residues. However, for reasons of protein stability and overall length of the experiment (>11 sec per scan) the irradiation time was not chosen longer.

Relaxation delays for $R_N(N_z)$ experiments on the CHAPS-free m^7GDP–eIF4E complex were 22.2, 88.8, 333, 610, 944, 1276, 1610, and 1887 ms. Delays for $R_N(N_z)$ experiments on the m^7GDP complex with 25 mM CHAPS and the apoprotein with 50 mM CHAPS were 22.2, 111, 333, 555, 833, 1110, 1498, and 1887 ms. Delays for the $R_N(N_z)$ experiments on the m^7GpppA complex with 50 mM CHAPS were 22.2, 88.8, 333, 610, 777, 999, 1610, and 1887 ms.

Delays for $R_N(N_{x,y})$ experiments on the CHAPS-free m^7GDP complex were 8.32, 16.64, 33.28, 49.92, 83.2, 116.7, and 133.1 ms. Delays for $R_N(N_{x,y})$ experiments on all CHAPS-containing complexes were 8.32, 16.64, 33.28, 49.92, 66.56, 83.2, 99.8, and 133.1 ms. The second time point in each $R_N(N_z)$ and $R_N(N_{x,y})$ series was repeated for error estimation.

Analysis of relaxation data

Spectra were processed using the FELIX software package (MSI/Biosym Inc.) and analyzed using XEASY (Bartels et al., 1995) on Silicon Graphics workstations. For sensitivity-enhanced relaxation data, the echo/antiecho pairs were added and subtracted to form complex points before processing (Cavanagh et al., 1991; Palmer et al., 1991; Kay et al., 1992; Cavanagh and Rance, 1993; Schleucher et al., 1994). The volume of each peak was determined by rectangular integration within XEASY. Extremely overlapped peaks were ignored.

The relaxation data were analyzed as described by Peng and Wagner (1992a,b). Decay curves were fitted to a single exponential function using the Levenburg–Marquadt nonlinear least-squares method. The resulting fits were graphed in PLOT (New Unit Inc., Ithaca, NY). Uncertainties in the $R_N(N_z)$ and $R_N(N_{x,y})$ rates were estimated using Monte Carlo simulations using one repeated time point as described by Peng and Wagner (1992a,b). The reduced spectral density was mapped using $R_N(N_{x,y})$, $R_N(N_z)$ and the heteronuclear NOE as described (Peng and Wagner, 1992a,b,1995; Ishima and Nagayama, 1995a,b). In the limit of fast internal motions, which is the case for amides locked into regular secondary structure, the $R_N(N_{x,y})/R_N(N_z)$ ratio depends only on τ_c (Kay et al., 1989). Anisotropic effects were not taken into account here because the conformation of the overall eIF4E/CHAPS complex is unknown, and the structure of eIF4E itself in the presence of CHAPS is fairly close to spherical (Matsuo et al., 1997). The quality of the CHAPS-free data is not very high. τ_c was calculated by fitting the $R_N(N_{x,y})/R_N(N_z)$ ratio via the Levenburg–Marquadt nonlinear least-squares method. The heteronuclear NOE experiment was recorded only once because of the limited stability of the protein under conditions of rf irradiation and the long duration of the experiment (>11 s per scan). Thus, no error limits were determined for the heteronuclear NOE and, consequently, no error limits are given for the spectral density functions.

Assignments for eIF4E within the CHAPS micelle were obtained in Matsuo et al. (1997). Assignments for CHAPS-free eIF4E were obtained from an HSQC titration with increasing CHAPS concentrations, and from a comparison of NOESY-HSQCs taken with and without added CHAPS.

HD exchange experiments

Since yeast eIF4E cannot be lyophilized to obtain a 100% D_2O sample, NH exchange experiments were performed by observing the decay of peak intensities in a 50% D_2O sample. A sample of m^7GDP-bound eIF4E containing 25 mM CHAPS was divided into two equal halves. This sample was prepared from media containing 99% D_2O. However, the sample was not used for HD exchange experiments until several weeks after the sample was made, allowing time for slowly exchanging amides to completely exchange back to ^{1}H before starting the experiments. One half of this sample was diluted to twice the original volume with H_2O buffer containing 25 mM CHAPS to record reference spectra. The other half was diluted to twice the original volume with D_2O buffer containing CHAPS at time $t = 0$, resulting in a 50% D_2O sample. HSQC spectra were acquired on the 50% D_2O sample at time $t = 0$, 8, 16, and 24 h. Reference spectra of the same length were taken on the 100% H_2O sample. The ratio of each peak volume in the 50% D_2O sample to the corresponding peak volume in the 100% H_2O reference sample was computed after each time point. The peak volume for a fully exchanged proton in the 50% D_2O sample will be half that of the corresponding peak volume in the reference spectrum. Decay curves were fit to the equation $I(t)/I_0 = 0.5e^{-t/R} + 0.5$ using the Levenburg–Marquadt nonlinear least-squares method. I_0 is the peak volume in the reference spectrum, I(t) is the peak volume after exchanging in 50% D_2O for time t, and R is the HD exchange rate.

Results

Relaxation parameters of the m^7GDP-bound eIF4E within the CHAPS micelle

We measured the longitudinal ($R_N(N_z)$) and transverse ($R_N(N_{x,y})$) relaxation rates, as well as the heteronuclear ^{1}H-^{15}N NOE (XNOE) to characterize the orientational dynamics of each ^{1}H-^{15}N bond and to map the spectral density functions, using uniformly ^{15}N-labeled, 99% deuterated eIF4E. Figure 2 (panel 1) shows the longitudinal and transverse relaxation

rates and the heteronuclear NOE enhancements for the m^7GDP-bound eIF4E with 25 mM CHAPS. Figure 3 (panel 1) shows the results of reduced spectral density apping for this sample.

The first 35 residues at the N-terminus of the protein are flexible and thus have slower transverse relaxation (see panel a1 of Figure 2), faster longitudinal relaxation (panel b1), and increased heteronuclear NOEs (panel c1) relative to the secondary structure elements of the protein. This increased flexibility leads to a greater proportion of high-frequency motions, reflected in the small values for $J_{eff}(0)$ and high values for $J(\omega_H)$ (see Figure 3, panel 1). The flexibility of the N-terminal region is evident in all three CHAPS-containing eIF4E complexes (see Figure 2, panels 1, 3, and 4).

Certain loops have increased mobility relative to the surrounding secondary structure elements, including the loops between b1 and a1, b3 and a3, b4 and a4, a5 and b7, and a6 and b8. These flexible loops are colored white in Figures 1a and b. These loop regions have a dip in $R_N(N_{x,y})$ and/or a rise in $R_N(N_z)$, accompanied by a dip in $J_{eff}(0)$ and/or a rise in $J_{eff}(\omega_H)$ and $J_{eff}(\omega_N)$, indicating a greater proportion of high-frequency motions (see Figure 2 (panel 1) and Figure 3 (panel 1)). The loop between b4 and a4 shows an unusually large degree of flexibility. These flexible loops include the loops preceding the two key tryptophan residues (Trp^{58} and Trp^{104}), which are primarily responsible for binding m^7GDP. Trp^{58} is located at the N-terminus of a1, close to the b1–a1 loop, and Trp^{104} is located within the b3–a3 loop, close to the N-terminus of a3. a1 and a3 are situated roughly perpendicular to the β-sheet in the concave inner face of eIF4E. The flexibility of these loops is consistent with the claim that the cap-binding site is not immersed in the CHAPS micelle, as initially indicated from the CHAPS titration experiments (Matsuo et al., 1997).

The loops between a2 and b3, and a4 and b5, which were predicted from the CHAPS titration to be embedded in the CHAPS micelle, do not show altered $R_N(N_z)$ or $R_N(N_{x,y})$ relative to the surrounding secondary structure regions, indicating either restricted flexibility due to contact with CHAPS, or some property of the protein itself which restricts mobility, such as hydrogen bonding. However, for the CHAPS-free m^7GDP complex, a prominent dip in $R_N(N_{x,y})$ for the loop between a2 and b3 confirms that the restricted flexibility seen for this loop in the CHAPS-containing complexes is due to the presence of the micelle (see Figure 2, panel a2). There were not enough clearly resolved peaks for the a4–b5 loop in the CHAPS-free sample to determine if the flexibility of this loop is also restored in the absence of CHAPS. These restrained loops are colored red in Figures 1a and b. Both loops are near helices a2 and a4, which are also thought to be embedded in the micelle.

Effects of different CHAPS concentrations on the relaxation parameters

To investigate how the detergent affects the mobility we performed experiments at three different CHAPS concentrations: 0, 25, and 50 mM. Figure 2 (panel 2) shows $R_N(N_{x,y})$, $R_N(N_z)$, and XNOE enhancements for CHAPS-free eIF4E with bound m^7GDP. Figure 3 (panel 2) shows the reduced spectral density mapping for this CHAPS-free eIF4E. Notice the difference in the average rates and overall correlation time (τ_c) between the CHAPS-containing and CHAPS-free samples (see Table 1). The m^7GDP-bound sample with 25 mM CHAPS is identical to the CHAPS-free sample except for its CHAPS concentration. The CHAPS-free sample has a τ_c of 11.8 ns, whereas the sample with 25 mM CHAPS has a τ_c of 15.9 ns. The large difference in overall correlation time indicates either the presence of a large CHAPS micelle or increased viscosity due to CHAPS in solution. In the CHAPS titration experiments, the changes in amide proton chemical shifts saturate at a CHAPS concentration of ~20–25 mM. Those residues showing chemical shift changes were mapped onto a contiguous region on one face of the eIF4E structure, indicating that this face is immersed in the CHAPS micelle (see Figures 1b and c).

The presence or absence of the mononucleotide or dinucleotide has no effect on the overall mobility of the protein. The sample used for measurements on the apoprotein and then for measurements on the m^7GpppA complex had a CHAPS concentration of 50 mM. There was no difference in average rates or overall correlation time between the apoprotein and the m^7GpppA complex, both in 50 mM CHAPS. Thus, the presence or absence of a bound cap analog has no significant effect on τ_c. As expected, comparison of the m^7GpppA complex in 50 mM CHAPS to the m^7GDP complexes in 0 and 25 mM CHAPS revealed large differences in overall correlation time (see Table 1). The 50 mM m^7GpppA complex has a τ_c of 19.4 ns, which is substantially longer than τ_c for the 25 mM m^7GDP complex (15.9 ns).

Only residues in the loop region between 199 and 206 show significant chemical shift changes between

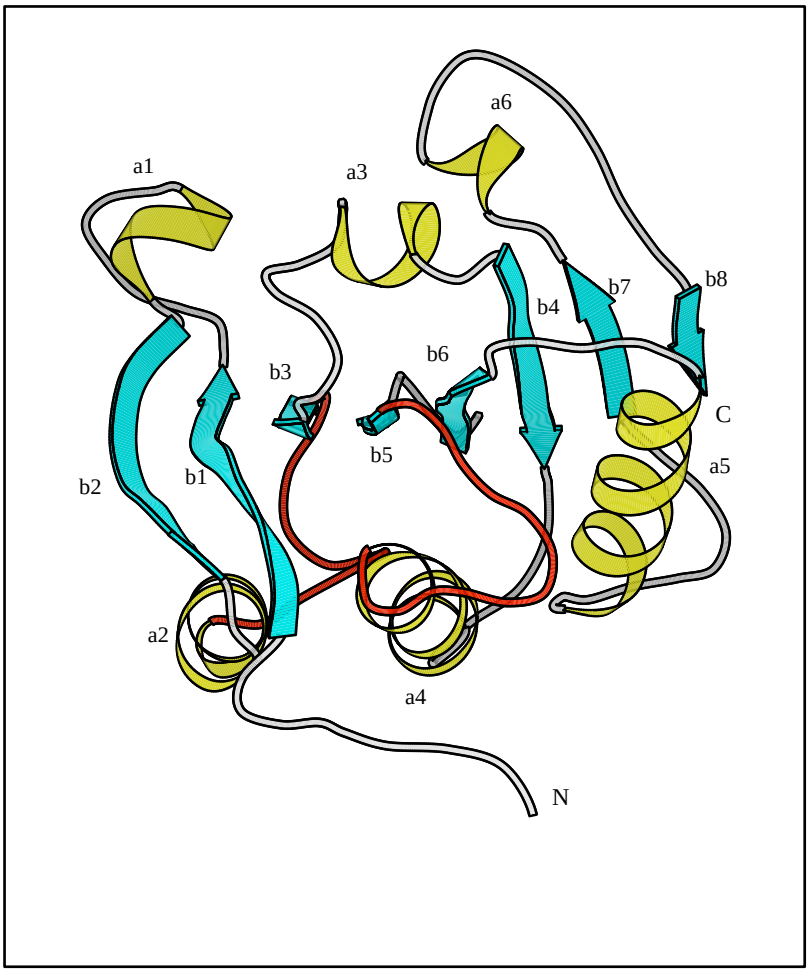

Figure 1. The eIF4E structure. (a) Molscript ribbon diagram of a representative structure. β-sheets are shown in blue and labeled b1–b8. α-helices are colored in yellow and labeled a1–a6. Loops that are flexible, based on relaxation data, are colored white, and loops that are rigid due to contact with the CHAPS micelle or due to interactions within the protein are colored red. Residues 1–37 are not shown as they are unstructured. (b) Ensemble of 20 backbone structures of yeast eIF4E viewed from the convex side of eIF4E away from the cap-binding site, containing the CHAPS-binding surface and the three long α-helices. The same coloring scheme as in part (a) is used here. (c) GRASP (Nicholls et al., 1991) surface representation of the region affected by the addition of CHAPS. Residues for which the amide ^{15}N or ^{1}H resonances shift by more than 0.5 or 0.1 ppm., respectively, are colored in yellow. Arrows indicate the three long helices. eIF4E is viewed from the same orientation as (b).

Table 1. Average relaxation parameters

Parameters[a]	No CHAPS (m^7GDP complex)	25 mM CHAPS (m^7GDP complex)	50 mM CHAPS m^7GppA complex)[b]
τ_c (ns)[c]	11.8	15.9	19.4
$R_N(N_{x,y})$ (s^{-1})	13.7	19.5	25.9
$R_N(N_z)$ (s^{-1})	1.3	1.0	0.9
$R_N(N_{x,y})/R_N(N_z)$	10.3	19.3	29.4

a These values were computed for the central structured core of eIF4E, excluding the first 35 unstructured residues at the N-terminus.

b The 50 mM sample was used for measurements on the apoprotein, followed by the addition of m^7GppA. Overall parameters for the 50 mM sample were approximately the same for the apoprotein and for the m^7GpppA-bound forms.

c τ_c is the overall correlation time.

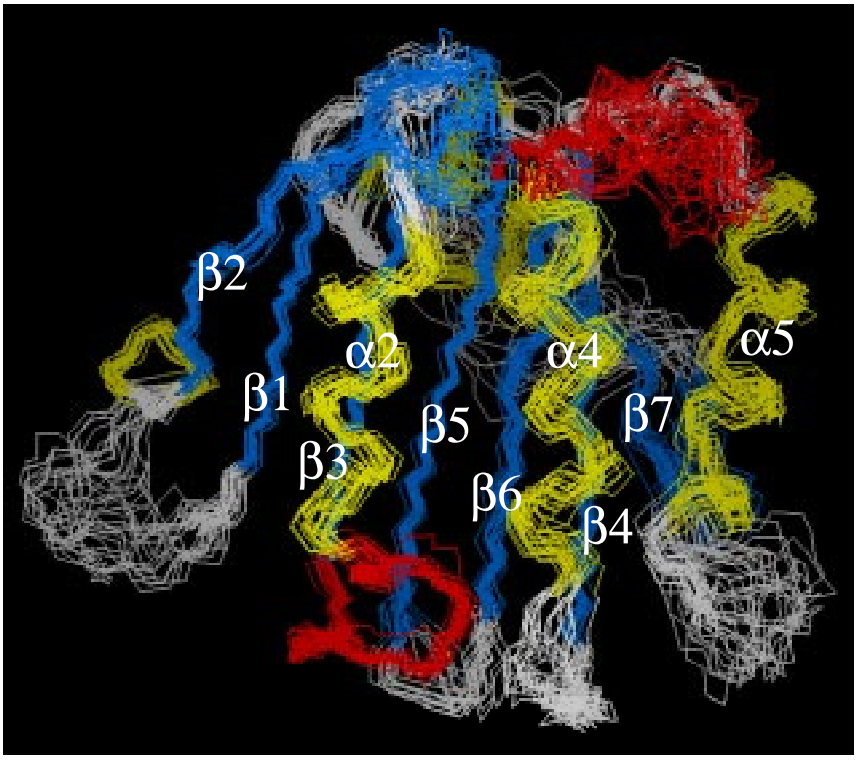

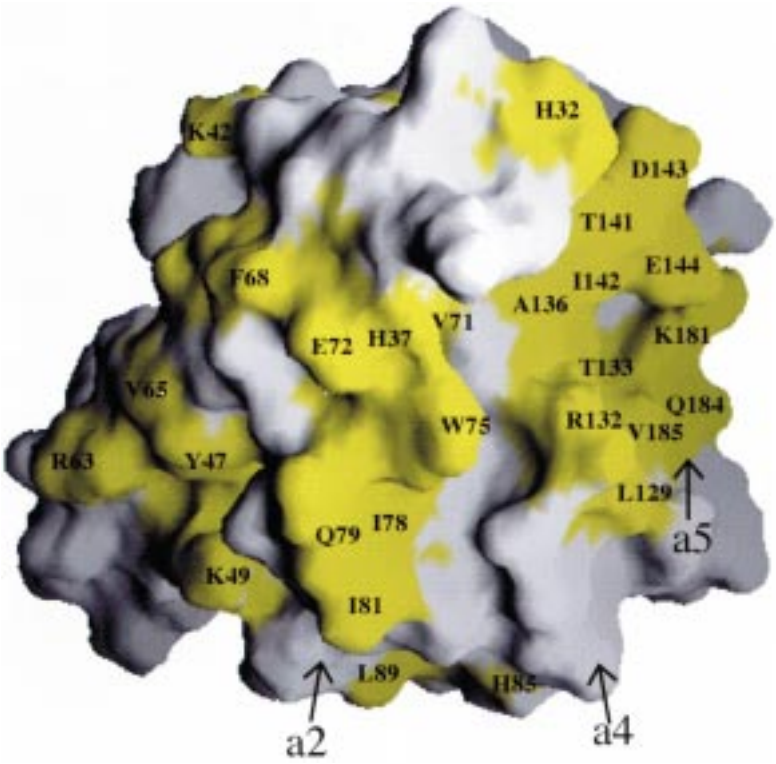

Figure 1. Continued.

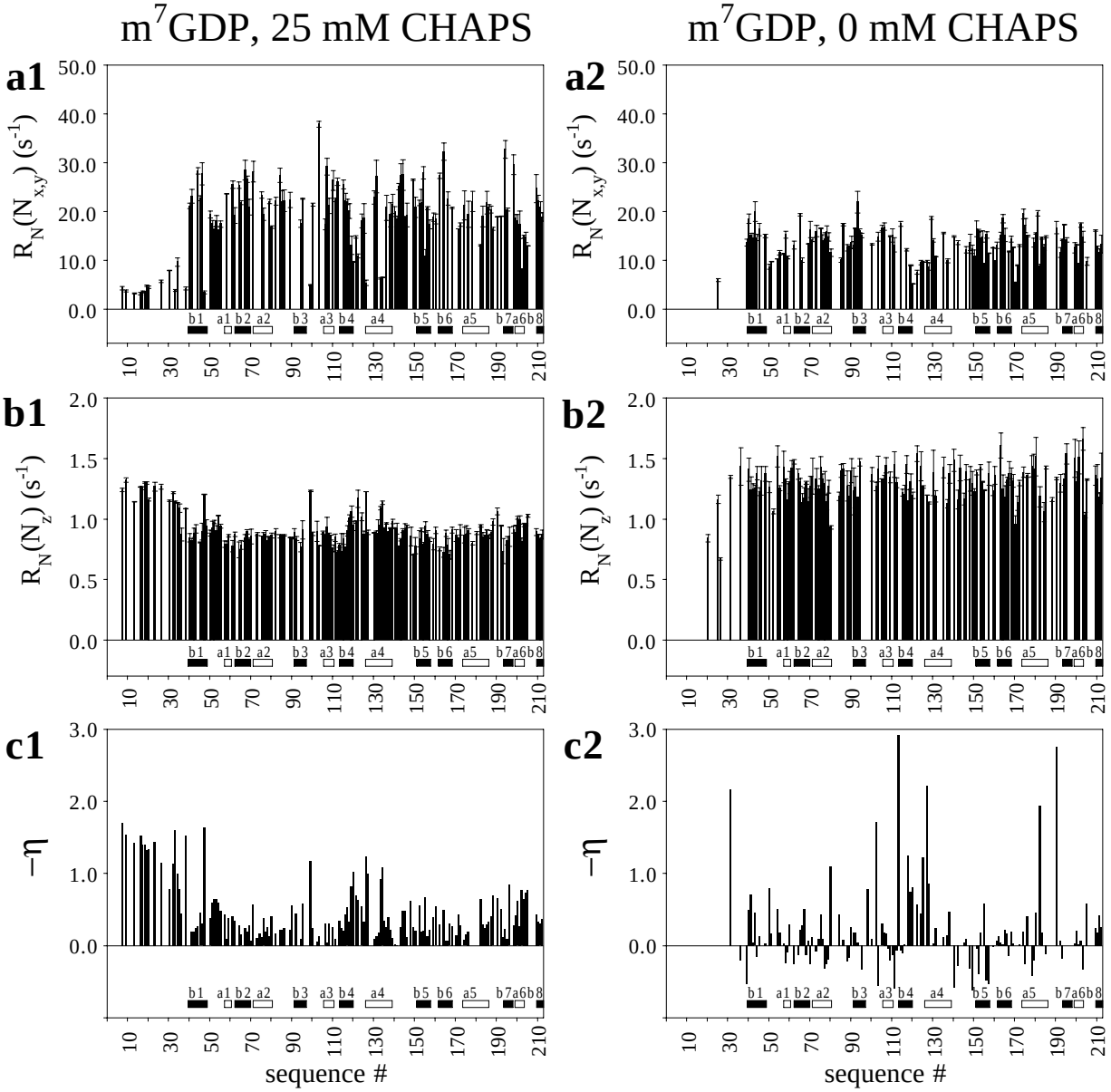

Figure 2. Relaxation rates and heteronuclear NOE enhancements for the four situations studied, measured at 500 MHz, 25 °C, 0.5 mM, and pH 6.5. (a) Relaxation rates for nitrogen transverse magnetization, $R_N(N_{x,y})$. (b) Relaxation rates for nitrogen longitudinal magnetization, $R_N(N_z)$. (c) The negative of the heteronuclear enhancement (XNOE) is plotted: $\eta = -(I_{sat}-I_0)/I_0$. eIF4E secondary structure elements are diagrammed across the bottom of the figure. Panel 1 shows relaxation data for the m^{7}GDP complex with 25 mM CHAPS, panel 2 shows data for the m^{7}GDP CHAPS-free complex, panel 3 shows data for the m^{7}GpppA complex with 50 mM CHAPS, and panel 4 shows data for the apoprotein with 50 mM CHAPS. Uncertainties in $R_N(N_{x,y})$ and $R_N(N_z)$ were estimated using Monte Carlo simulations with one repeated time point as described by Peng and Wagner (1992a,b).

the m^{7}GDP- and m^{7}GpppA-bound forms, and the secondary structure elements in the m^{7}GpppA complex seem to have the same relative dynamic properties as in the m^{7}GDP-bound form (see Figure 2 (panel 3) and Figure 3 (panel 3)). Therefore, we can conclude that the differences in overall correlation time between the m^{7}GDP- and m^{7}GpppA-bound eIF4E are due to the presence of either a larger micelle with 50 mM CHAPS than with 25 mM CHAPS, or increased viscosity due to an increased amount of CHAPS in solu-

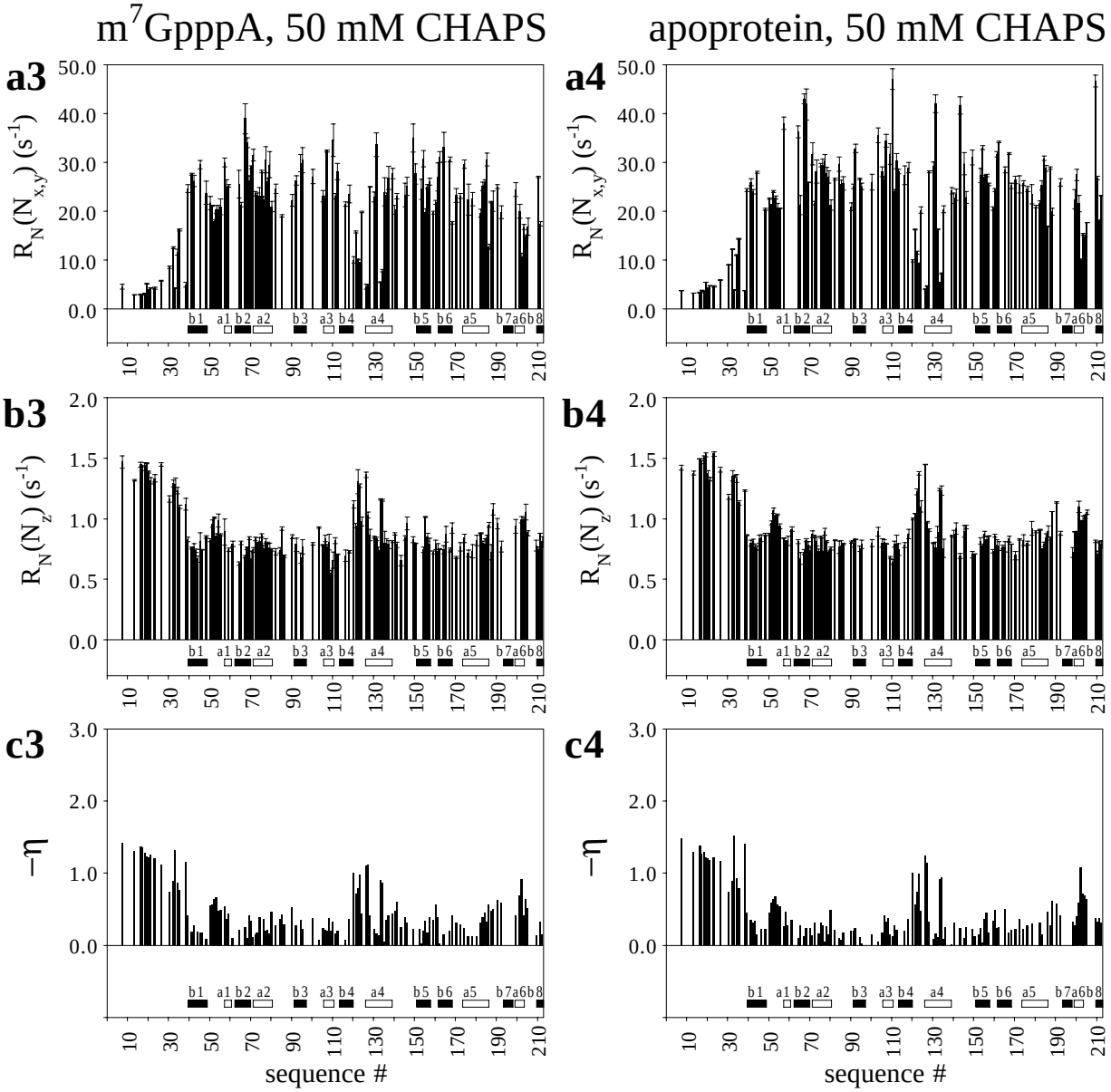

Figure 2. Continued.

tion. Thus, varying the concentration of CHAPS over the range of 25–50 mM has a substantial effect on the overall correlation time. Based on our dynamic light scattering data and a compilation of all experimentally determined correlation times for proteins of different sizes (Dayie et al., 1996; Wagner, 1997), we can estimate that the molecular weight of the CHAPS micelle found containing the protein at 25 mM CHAPS must be around 40–60 kDa.

Because the yeast eIF4E is less soluble in the absence of CHAPS, relaxation measurements on eIF4E without added CHAPS were taken at lower concentration (<0.5 mM). In addition to this, gradual accumulation of unfolded protein led to substantial overlap in the center of the spectrum. Data from many residues in the central part of the spectrum (∼7.7–8.6 ppm for ^{1}H and ∼118–128 ppm for ^{15}N) could not be used due to overlap with unfolded protein. This included most of the amides in the unstructured N-terminus of

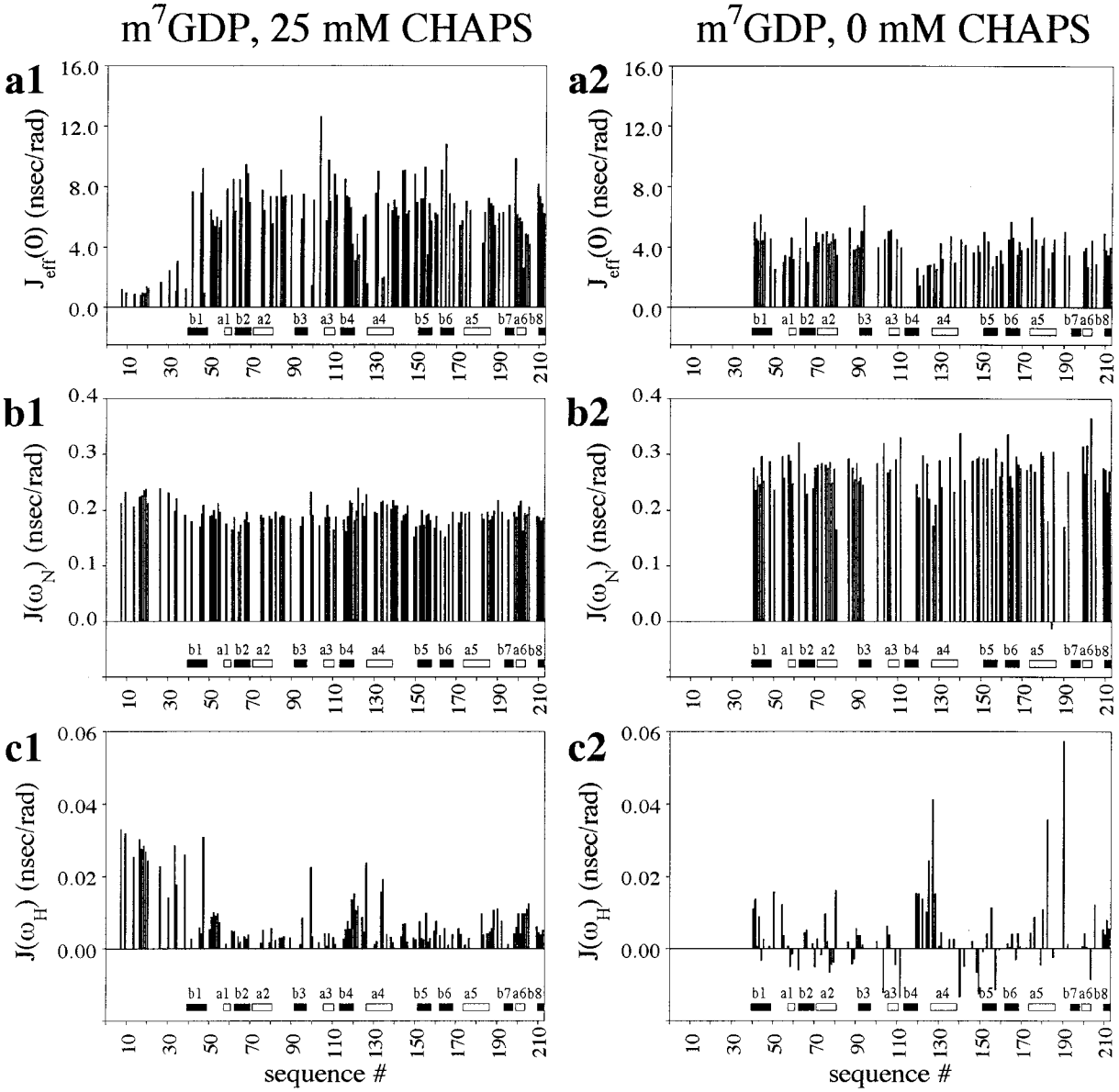

Figure 3. Reduced spectral density mapping for the four situations studied, calculated from the $R_N(N_{x,y})$, $R_N(N_z)$, and XNOEs shown in Figure 2. (a) $J_{eff}(0)$. (b) $J(\omega_N)$.(c) $J(\omega_H)$. Panel 1 shows the results of reduced spectral density mapping for the m^7GDP complex with 25 mM CHAPS, panel 2 shows the mapping for the m^7GDP CHAPS-free complex, panel 3 shows the mapping for the m^7GpppA complex with 50 mM CHAPS, and panel 4 shows the mapping for the apoprotein with 50 mM CHAPS.

the protein (residues 1–35), as well as other residues throughout the protein, especially in the loop regions (see Figure 2, panel 2). Relaxation rates were calculated for only a few residues in the unstructured N-terminus. The $R_N(N_z)$ spectra were recorded first and the rates for four residues in this region could be calculated (see Figure 2, panel 2b). By the time the XNOE spectra were recorded 5 days later, three of these four residues were no longer resolved (see Figure 2, panel 2c) and the signal-to-noise was substantially reduced. This is also due to the lower sensitivity of the XNOE experiments. Because of lower signal-to-noise in the CHAPS-free sample and the resulting error in the rates, it is difficult to draw conclusions about individual residues from these data.

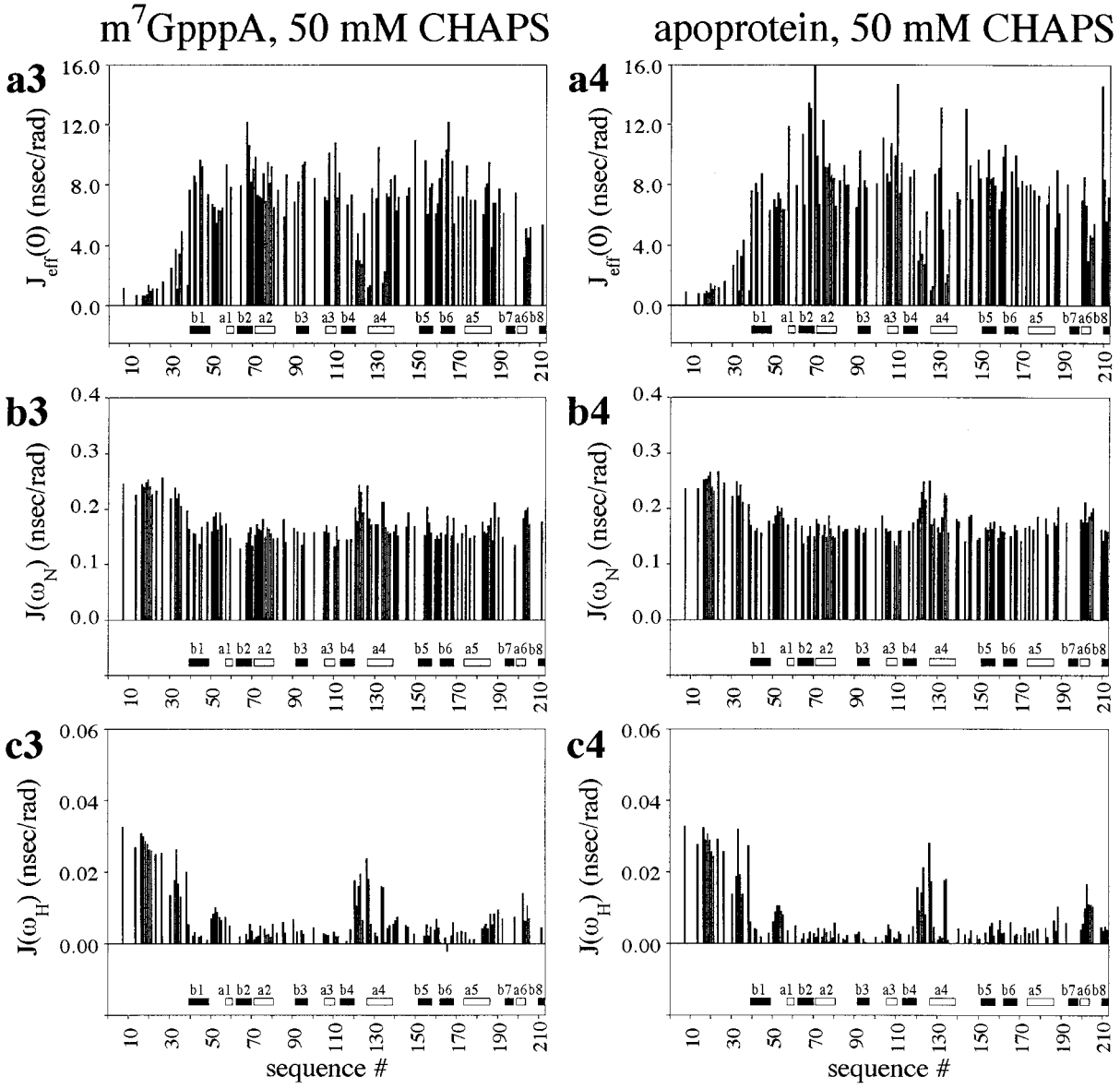

Figure 3. Continued.

Comparison of apoprotein, m^{7}GpppA-, and m^{7}GDP-bound eIF4E in the CHAPS micelle

To investigate the effects of different cap analogs on the mobility of eIF4E in the CHAPS micelle, we compared relaxation rates for the apoprotein and for the m^{7}GDP and m^{7}GpppA eIF4E complexes. Since the apoprotein and the m^{7}GpppA complex contain the same CHAPS concentration, mobility differences upon binding of the cap analog can be compared. Figure 2 (panel 3) shows the relaxation data for the m^{7}GpppA complex, and Figure 2 (panel 4) shows the relaxation data for the apoprotein. Figure 3 (panels 3 and 4) shows the reduced spectral density mapping for these two situations. Comparison of relative relaxation rates for the different secondary structure elements indicates that the same dynamic properties are present in both the apoprotein and the m^{7}GpppA-bound forms.

Because the CHAPS concentration was identical in the dinucleotide complex and the apoprotein, all data points in a plot of a dinucleotide relaxation parameter ($R_N(N_{x,y})$, $R_N(N_z)$, or XNOE) versus the corresponding parameter in the apoprotein should lie on the line

$y = x$, except for those residues with locally altered mobility due to the presence of the bound cap analog (see Figure 4, panel 1). For all three parameters, the least squares fit for the datapoints in these plots is close to the line $y = x$, with $\chi^2 \geq 0.93$. There are no significant outliers, and there are no significant anomalies in the rates of those residues known to be involved in the interaction with the dinucleotide. Figure 4 (panel 2) shows plots of the relaxation parameters for the m^7GDP-bound eIF4E versus the corresponding parameter for the apoprotein. These two samples have different CHAPS concentrations; hence, the best fits to these points do not have a slope of 1 or a y-intercept of 0. This shows the 'scaling' of the rates due to the presence of the CHAPS micelle.

No significant anomalies were seen in the relaxation rates of the three forms bound in the CHAPS micelle. The same general features are present in the relaxation data for all three forms (see Figure 2, panels 1, 3, and 4); the results are simply 'scaled' by the difference in correlation time due to the difference in CHAPS concentration. The dips in $R_N(N_{x,y})$, corresponding to flexible loops with greater internal mobility, show up in the same locations in the eIF4E sequence in all three data sets, but the magnitudes of the rates in each data set are scaled by the difference in correlation time, which is due to the difference in the CHAPS concentration. In addition, comparing the relaxation parameters of the side-chain NεH cross peaks for the eight tryptophan side chains also shows no significant changes which cannot be accounted for by the difference in CHAPS concentration.

It was impossible to measure the relaxation rates of certain residues surrounding the cap-binding site of the apoprotein because these residues disappear or remain unassigned in the apoprotein. NH cross peaks for His^{94}, Glu^{103}, Glu^{105}, Val^{153}, Leu^{165}, as well as the side chain NεH of Trp^{166} disappear in the apoprotein. These residues are all known to form NOE contacts with, or be adjacent to, residues which contact m^7GDP. If these resonances are unobservable due to broadening in the apoprotein, this could indicate microsecond to millisecond motion near the intermediate exchange regime. However, it is likely that these resonances simply shift position in the apoprotein spectra and we do not yet have all the assignments for the apoprotein. Cross peaks which shift less dramatically, for which we were able to measure the relaxation rates, include the amides of Thr^{48}, Trp^{58}, Leu^{62}, Lys^{158}, Trp^{104}, and Trp^{166}, and the side-chain NεH crosspeak of Trp^{104}. For these residues, there were no significant changes in the relaxation rates which are not accounted for by the difference in CHAPS concentration.

Resonance shifts upon the addition of m^7GpppA were mostly confined to the loop-containing region from 199 to 206. While His^{199}, Ser^{201}, Asn^{203}, and Lys^{114} remain unassigned in the m^7GpppA-bound protein, Ser^{200} and Ala^{202} shift but can be followed. For these residues, there is no substantial change in the relaxation rates between the apoprotein and the m^7GpppA-bound form. In addition, the new peaks which appear in the spectrum of the dinucleotide-bound form, although unassigned, have relaxation rates similar to typical values in this loop region in the apoprotein form.

Amide hydrogen exchange experiments

The amide hydrogen exchange data are also consistent with the presence of a CHAPS micelle. Figures 5a and b show the ratios of HSQC peak volumes of a 50% D_2O sample to an H_2O sample with the same protein concentration at two different time points (8 and 24 h). A value of 1.0 indicates no exchange, and a value of 0.5 indicates full exchange. Amide hydrogen exchange rates could be calculated for 34 residues. Figure 5c plots these rates as a function of sequence. Fast exchanging amides which were completely exchanged in the first experiment are indicated by a dot on the line at $y = 0$ h. Amides exchanging too slowly for their rates to be measured in our experiments (rates ≥ 60 h) are plotted as dots on the line at $y = 60$ h.

Hydrogen exchange was measured at pH 6.5 and at 25 °C. Under these conditions, random coil peptides have exchange rates in the range of 1 s^{-1}. Thus, all residues that have a value >0.5 in Figure 5a have amide protons protected from solvent access. Most of the loops show rapid exchange before the first time point, whereas most secondary structural elements show little exchange when the final experiment was completed after 32 h. There is some additional exchange that occurs between the 8 h time point and the 32 h time point, for instance in b2 and the b3–a3 and a4–b5 loops. The rates for these residues are plotted in Figure 5c. The regions that are the most structured or protected by CHAPS retain ~80–90% of their signal intensity after 32 h (see Figure 5b). These residues are indicated in Figure 5c with dots on the line at $y = 60$ h. Significant intensity in these regions remained after several days.

The two surface-exposed α-helices predicted from the CHAPS titration to be immersed in the CHAPS

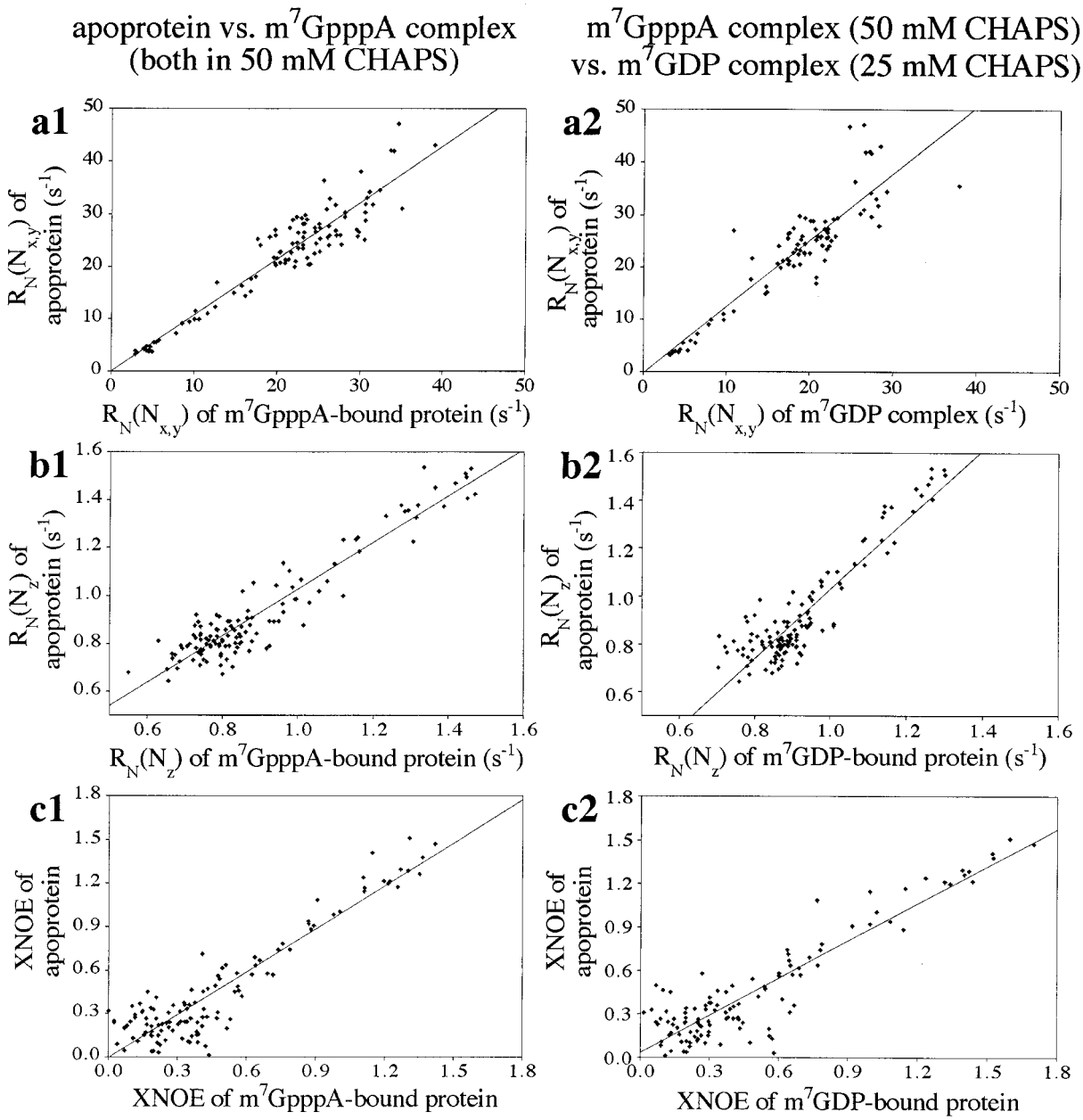

Figure 4. (a1–c1) Plots of relaxation parameters for the m^7GpppA complex versus the corresponding parameter in the apoprotein for each residue. Because both samples have the same CHAPS concentration and there is no significant difference in mobility between these two forms, the points fall close to the line y = x. (a1) $R_N(N_{x,y})$. The best fit line is $y = 0.009 + 1.07x$, $\chi^2 = 0.95$. (b1) $R_N(N_z)$. The best fit is $y = 0.05 + 0.97x$, $\chi^2 = 0.94$. (c1) XNOE. The best fit is $y = -0.01 + 0.99x$, $\chi^2 = 0.93$. (a2–c2) Plots of relaxation parameters for the m^7GDP-bound complex versus the corresponding parameter in the apoprotein. The CHAPS concentration is different for these two samples and therefore the slope $\neq 1$ and the y-intercept $\neq 0$ for the best fit line. (a2) $R_N(N_{xy})$. The best fit is $y = -0.26 + 1.27x$, $\chi^2 = 0.91$. (b2) $R_N(N_z)$. The best fit is $y = -0.42 + 1.45x$, $\chi^2 = 0.91$. (c2) XNOE. The best fit is $y = 0.03 + 0.86x$, y, $\chi^2 = 0.91$.

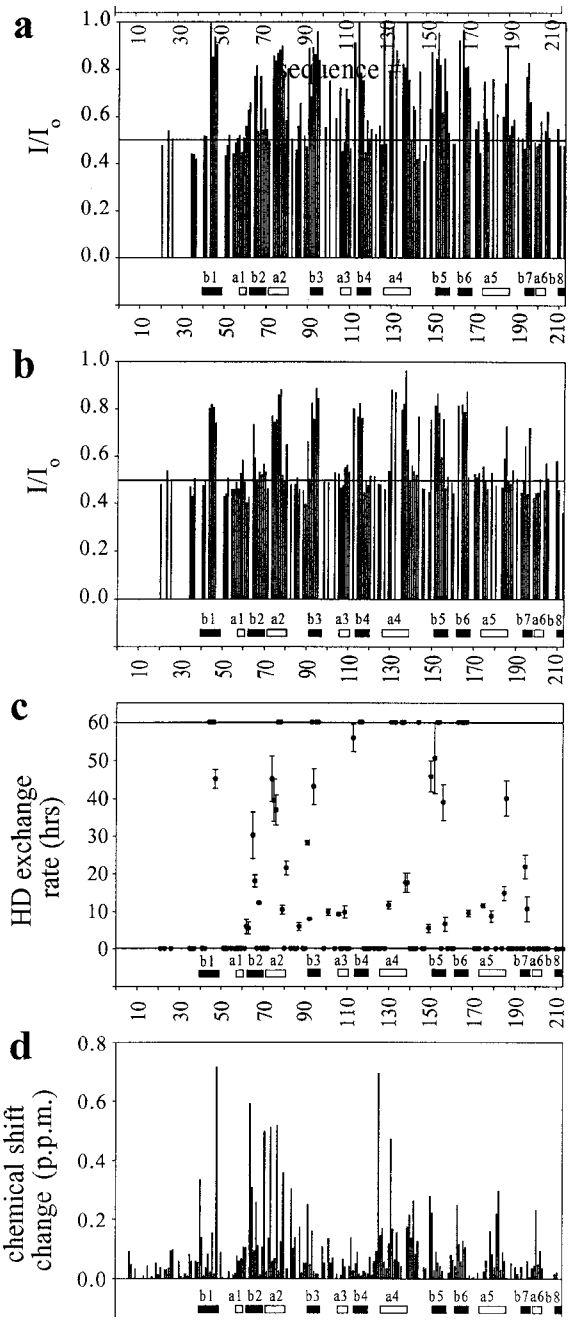

Figure 5. Amide hydrogen exchange and CHAPS titration chemical shift changes plotted versus protein sequence. Ratios of HSQC peak volumes between a reference H_2O sample and a sample exchanging in 50% D_2O (I/I_0) after (a) 0–8 h and (b) after 24 h. A value of 1.0 corresponds to no exchange; a value of 0.5 corresponds to full exchange. (A line is drawn to indicate a value of 0.5.) (c) HD exchange rates as a function of sequence . Residues with rates too fast to be measured (amides that are completely exchanged after 8 h) and residues that exchange rapidly but gave poor fits are plotted on the line at $y = 0$. Residues with exchange rates too slow to be measured ($\geq$60 h) are plotted on the line at $y = 60$ h. Uncertainties in the rates are obtained from the Levenburg–Marquadt nonlinear least-squares fits. (d) Chemical shift changes in the CHAPS titration. The ^1H chemical shift change added to 20% of the ^{15}N chemical shift change is plotted as a function of sequence. The secondary structure shown at the bottom.

micelle, a2 and a4, show very little exchange in 32 h. Phe^{74}, Trp^{75}, and Ala^{76} in a2 have exchange rates of 45.1, 39.6, and 37.0 h, respectively. Ile^{77} and Ile^{78} in a2 have exchange rates longer than the range of our measurements ($\geq$60 h). Leu^{131}, Thr^{133}, Ala^{136}, and Val^{137} in a4 also have very slow rates ($\geq$ 60 h).

All of the other surface-exposed helices in eIF4E are fully exchanged after 32 h. The presence of a CHAPS micelle coating this side of the protein and protecting helices a2 and a4 from solvent exchange could explain the difference in amide hydrogen exchange rates between these two helices and the other four helices in the protein. Another possibility is the presence of a stabilizing intraprotein interaction in these two helices; however, we know from the CHAPS titration that these two helices show some of the largest chemical shift changes in the protein. Thus, the solvent protection is more likely a result of immersion in the CHAPS micelle. The four rapidly exchanging helices include a1 and a3, which contain or are close to the two key cap-binding tryptophan residues, Trp^{58} and Trp^{104}, because the cap binding site is not immersed in the micelle. Figure 5d shows the chemical shift changes observed in the CHAPS titration.

The a4–b5 loop, which is predicted to be immersed in the CHAPS micelle based on the relaxation data and the CHAPS titration, does contain slowly exchanging residues. After 8 h, there is still some intensity for Thr^{141}, Asp^{143}, and Glu^{144}, but these residues are fully exchanged after 32 h. These residues did not give good enough fits to calculate exchange rates. This region also shows significant chemical shift changes in the CHAPS titration (see Figure 5d). The a2–b3 loop is also predicted to be immersed in the micelle; however, this loop does not show dramatically increased protection on the time scale of these experiments.

The b3–a3 loop and the adjacent helix a3 also seem to have several relatively slowly exchanging residues; there is still some intensity remaining after 8 h in residues Arg^{101}, Asp^{106}, Asn^{109}, and Ala^{110}, but these residues are completely exchanged after 32 h. Exchange rates for Arg^{101}, Asp^{106}, and Asn^{109} are 9.8, 9.3, and 99 h, respectively. The loop consists of residues 97–105, including Trp^{104}, which together with Trp^{58} sandwiches the methylated cap analog in the structure. Thus, the slowly exchanging residue Arg^{101} is contained within this loop, and it is likely that Arg^{101} is involved in a hydrogen bonding interaction. Unfortunately, there was overlap or not enough signal intensity to measure the HD exchange ratio for other residues in this flexible loop region, including Glu^{105} and Glu^{103}. The side chains of Glu^{105} and Glu^{103} are known to form hydrogen bonds with the amino group of the m^{7}G of the cap analog and NεH of Trp^{58}, respectively.

It would be interesting to compare our amide hydrogen exchange data recorded in the presence of CHAPS to the corresponding experiments performed using CHAPS-free eIF4E. This would be much more difficult, however, due to the fact that CHAPS-free eIF4E precipitates at high concentration. In addition to starting from a substantially lower concentration, the original sample must be diluted twofold with D_2O before recording the data, reducing the sensitivity even further.

Discussion and Conclusions

We have studied the dynamics and amide hydrogen exchange of yeast eIF4E immersed in a CHAPS micelle, with two different concentrations of CHAPS, as well as in the CHAPS-free form. The overall correlation times of the CHAPS-free protein and the protein–micelle complexes with two different CHAPS concentrations are very different. We conclude that in the presence of 25–50 mM CHAPS, eIF4E is part of a large CHAPS micelle whose size depends on the CHAPS concentration. Because of the low critical micelle concentration for CHAPS (6 mM), dynamic light scattering data, and comparison of our measured correlation times to other published protein correlation times, we estimate that the size of the micelle is somewhere in the range of 40–60 kDa at the CHAPS concentrations used in these experiments. Since the molecular weight of yeast eIF4E itself is only 24.3 kDa, this implies that the eIF4E–CHAPS micelle contains between 25 and 60 molecules of CHAPS (the molecular weight of CHAPS is 0.612 kDa).

Our data support a model in which the convex surface of eIF4E is immersed in the CHAPS micelle, including helices a2 and a4, β-strands b1 and b2, and the a2–b3 and a4–b5 loops. The concave surface of eIF4E, including the cap-binding site, does not seem to be in contact with the micelle. Helices a2 and a4 show substantial chemical shift changes in the CHAPS titration experiments. These helices have very slowly exchanging amide protons compared to all the other helices in the protein, consistent with protection due to immersion in a micelle. Approximately 80–90% of the original signal intensity of the most protected secondary structure elements remains after 24 h, and

some amide signal intensity remains after several days. The relaxation and amide hydrogen exchange experiments provide additional evidence for the a2–b3 and a4–b5 loops being in contact with the micelle. These two loops show reduced mobility relative to the other loops in the structure for the CHAPS-containing samples. However, the a2–b3 loop appears to be flexible in the absence of CHAPS, indicating that the reduced mobility is due to the CHAPS micelle and not some internal feature of the protein itself. The a4–b5 loop shows increased protection from solvent on the time scale of 8 h.

Our data support the idea that the cap-binding site is situated outside of the micelle. Residues surrounding the cap-binding site do not show large chemical shift changes in the CHAPS titration, and the binding of cap analogs is unaffected by the presence of CHAPS. In addition, the loops preceding the two critical tryptophan residues, Trp^{58} and Trp^{104}, appear to be flexible, both in the apoprotein and with bound cap analog.

In addition, our data suggest a mode of cap analog binding which does not cause substantial change in the mobility of binding site residues. The general dynamic features of the binding-site loops remained unchanged in the apoprotein, m^7GDP-, and m^7GpppA-bound forms. In the m^7GpppA titration, chemical shift changes were confined to the region between residues 199 and 206. The flexible loop within this region does not seem to become more structured upon binding m^7GpppA. The overall correlation times were different in the samples used due to different CHAPS concentrations; however, general features of the internal dynamics were unchanged despite the significantly different correlation times. The overall magnitudes of the relaxation rates scale with the overall correlation time, but the relative mobilities of secondary structure elements within each sample remain the same. We were unable to draw conclusions about those residues within the cap-binding site which disappear or shift substantially in the apoprotein or the dinucleotide complex, as assignments are only known for m^7GDP-bound eIF4E and several key residues disappear or remain unassigned.

An interesting feature of the relaxation data is the unusually high mobility present in the loop between b4 and a4 in all four forms, both in the presence and absence of CHAPS (see Figure 2). There is a very pronounced increase in $R_N(N_z)$ and XNOE, and a dip in $R_N(N_{x,y})$ for the area surrounding this loop. The rise in $R_N(N_z)$ is particularly prominent for the two 50 mM CHAPS samples (see Figure 2, panels 3 and 4). The rise in the magnitude of the XNOE is evident in all four samples. In addition, there is abnormally increased mobility in the center of the adjacent helix a4. The mobility of this loop region seems to be unaffected by the presence of the CHAPS micelle. From the CHAPS titration data, this loop seems to be relatively unaffected by CHAPS binding; however, the adjacent helix a4 shows very large chemical shift changes, starting with Asp^{127}, which is very close to this loop.

The apparent increased mobility for this loop region is surprising, given that this is a rather short loop, encompassing residues 120–125. It shows even greater mobility than the b1–a1 loop, which is twice as long. In the eIF4E structure in the presence of CHAPS, this loop appears to be restricted because of its short length. However, there are many ^{1}H-^{1}H side-chain to amide NOEs between helix a4 and the β-sheet between residues 130 and 138, but few NOEs in the region adjacent to this loop, between 126 and 129. Surprisingly, Leu^{129} and Ile^{126}, which both point towards the interior of the molecule, do not have any NOEs to the β-sheet. Perhaps this end of the helix is not held as rigidly against the β-sheet, allowing for greater flexibility in this short loop.

Our data suggest that there is no dramatic change in the structure or relative mobilities of secondary structural elements of eIF4E between the CHAPS-free protein and the protein immersed in the CHAPS micelle. Other than mobility changes in several surface-exposed loops, the overall structure remains essentially unchanged, as indicated by small changes in the NMR spectra upon the addition of CHAPS. Addition of the non-denaturing detergent CHAPS could be a promising technique for increasing the solubility and stability of other difficult proteins.

Acknowledgements

We thank Greg Heffron for assistance with NMR spectroscopy, Jeffrey Peng for providing his analysis programs for relaxation, and Nahum Sonenberg and Anne-Claude Gingras for providing the yeast eIF4E construct and the m^7GDP affinity resin. This work was supported in part by the National Institute of Health (G.W.), the National Science Foundation (G.W.), and the Harvard Center for Structural Biology and the Giovanni Armenise-Harvard Foundation for Advanced Scientific Research (G.W.). A.M.M. is a

Howard Hughes Medical Institute Predoctoral Fellow. H.M. acknowledges partial support from the Toyobo Biotechnology Foundation.

References

Bartels, C., Xia, T.-H., Billeter, M., Güntert, P., and Wüthrich, K. (1995) *J. Biomol. NMR*, **6**, 1–10.

Cavanagh, J., Palmer III, A.G., Wright, P.E. and Rance, M. (1991) *J. Magn. Reson.*, **91**, 429–436.

Cavanagh, J. and Rance, M. (1993) *Annu Rep. NMR Spectrosc.*, **27**, 1–58.

Chattopadhyay, A. and Harikumar, K.G. (1996) *FEBS Lett.*, **391**, 199–202.

Dayie, K.T., Wagner, G. and Lefèvre, J.F. (1996) *Annu. Rev. Phys. Chem.*, **47**, 243–282.

Edery, I., Altmann, M. and Sonenberg, N. (1988) *Gene*, **74**, 517–525.

Farrow, N.A., Muhandiram, R., Singer, A.U., Pascal, S.M., Kay, C.M., Gish, G., Shoelson, S. E., Pawson, T., Forman-Kay, J.D., and Kay, L.E. (1994) *Biochemistry*, **33**, 5984–6003.

Haghighat, A., Mader, S., Pause, A. and Sonenberg, N. (1995) *EMBO J.*, **14**, 5701–5709.

Ishima, R. and Nagayama, K. (1995a) *Biochemistry*, **34**, 3162–3171.

Ishima, R. and Nagayama, K. (1995b) *J. Magn. Reson.*, **B108**, 73–76.

Kay, L.E., Torchia, D.E. and Bax, A. (1989) Biochemistry, 28, 8972–8979.

Kay, L.E., Keifer, P. and Saarinen, T. (1992) *J. Am. Chem. Soc.*, **114**, 10663–10665.

Kraulis, P.J. (1991) *J. Appl. Crystallogr.*, **24**, 946–950.

Marcotrigiano, J., Gingras, A.-C., Sonenberg, N., and Burley, S.K. (1997) *Cell*, **89**, 951–961.

Matsuo, H., Li, H., McGuire, A. M., Fletcher, C. M., Gingras, A.-C., Sonenberg, N. and Wagner G. (1997) *Nat. Struct. Biol.*, **4**, 717–724.

Merrick, W.C. and Hershey, J.W.B. (1996) *In Translational Control* (Eds., Hershey, J.W.B., Mathews, M.B. and Sonenberg, N.), Cold Spring Harbor Laboratory Press, Plainview, New York, NY, pp. 31–69.

Nicholls, A., Sharp, K.A. and Honig, B. (1991) *Proteins*, **11**, 281–296.

Nirmala, N. R. and Wagner, G. (1988) *J. Am. Chem. Soc.*, **110**, 7557–7558.

Nirmala, N.R. and Wagner, G. (1989) *J. Magn. Reson.*, **82**, 659–661.

Palmer III, A.G., Cavanaugh J., Wright, P.E. and Rance, M. (1991) *J. Magn. Reson.*, **93**, 151–170.

Peng, J.W. and Wagner, G. (1992a) *J. Magn. Reson.*, **98**, 308–332.

Peng, J.W., and Wagner, G. (1992b) *Biochemistry*, **31**, 8571–8586.

Peng, J. W. and Wagner, G. (1995) *Biochemistry*, **34**, 16733–16752.

Schleucher, J., Schwendinger, M., Sattler, M., Schmidt, P., Schedletzky, O., Glaser, S.J., Sørenson, O.W., Griesinger, C. (1994) *J. Biomol. NMR*, **4**, 301–306.

Wagner, G. (1997) *Nat. Struct. Biol.*, **4**, 841–844.